Acta Sci. Pol.
Architectura 23 (2024), 1–11
aspa.sggw.edu.pl ISSN 1644-0633 (suspended) eISSN 2544-1760 DOI: 10.22630/ASPA.2024.23.1

ORIGINAL PAPER

Received: 28.12.2023
Accepted: 18.01.2024

HYDRAULIC CONDUCTIVITY TENSOR OF ANISOTROPIC SOILS: THE IMPACT ON SEEPAGE FLOW

Md Khorshed Alam[1]✉, Arvin Farid[2]

[1]Computing Ph.D. Program, Boise State University, Boise, ID, USA
[2]Department of Civil Engineering, Boise State University, Boise, ID, USA

ABSTRACT

Natural or artificial changes in soil stratigraphic-plane (i.e., the deposition of soil and sediments into distinct layers) orientation can cause variations in hydraulic conductivity in different directions. Hydraulic conductivity must, therefore, be considered – in this case – as a nondiagonal, full tensor to appropriately represent the effect of the orientation of soil stratigraphic planes on the seepage flow pattern. This paper introduces the derivation of the formula for the three-dimensional nondiagonal hydraulic conductivity full tensor calculation in terms of azimuth and vertical angles. Furthermore, two-dimensional numerical simulations of the seepage flow beneath a concrete dam are presented to demonstrate the need to account for the nondiagonal elements of the hydraulic conductivity tensor in anisotropic soils of varying degrees of stratigraphic tilt with respect to the coordinate system.

Keywords: full tensor, hydraulic conductivity, seepage flow, soil stratigraphy, numerical simulation

INTRODUCTION

Particle orientation, compaction, illuviation and sedimentation are some soil-forming processes that can cause anisotropy in any soil (Assouline & Or, 2006; Peng, 2011). Certain natural soils possess substantial anisotropy, resulting in significant variations in their mechanical or physical characteristics in various directions. This tendency is especially noticeable in clayey soils compared to other soil types (Nguyen, Rahman & Karim, 2023). Anisotropic soils may exhibit varying transport characteristics depending on the direction of principal flow and directional hydraulic conductivity. Therefore, analysis of seepage flow through anisotropic soils might necessitate tensorial representation instead of the scalar values of hydraulic conductivity observed in isotropic soils (Assouline & Or, 2006). In anisotropic soils, the permeability of the porous medium in various directions is described by the hydraulic conductivity tensor, a matrix that depends on the flow direction and soil stratigraphy – the deposition of soil and sediments into distinct layers. The hydraulic conductivity tensor has conventionally been regarded as diagonal, which signifies that the permeability remains unaffected by the flow direction. This assumption, nevertheless, might not apply to anisotropic soil – a medium in which permeability can vary substantially in various directions – where the principal directions of hydraulic conductivity differ from the system of coordinates used for flow simulation. One instance of this is the fluid-flow equations utilised to model numerous commercial reservoirs (Ertekin, Abou-Kassem & King, 2001; Fanchi, 2005). These equations operate under the supposition that nondiagonal elements of the tensor can be disregarded, leading to

Md Khorshed Alam https://orcid.org/0000-0002-1227-002X; Arvin Farid https://orcid.org/0000-0002-2832-3819
✉mdkhorshedalam@u.boisestate.edu

inaccurate flow calculations (Fanchi, 2008). Thus, Fanchi (2008) introduced a formula that enabled the precise computation of a two-dimensional full-hydraulic conductivity tensor, including nondiagonal components, at any rotation angle in a plane. In a subsequent study, Alam and Farid (2023) derived and utilised a similar formula to conduct numerical simulations of seepage in unsaturated soil. They investigated multiple scenarios using two-dimensional models and demonstrated that neglecting nondiagonal factors leads to erroneous seepage flows. Nonetheless, a three-dimensional model is needed to simulate more realistic circumstances, necessitating the development of a formula for the three-dimensional nondiagonal hydraulic conductivity full tensor, subject to the soil stratigraphic planes' tilt angle.

This paper presents a novel set of formulas to compute the diagonal and nondiagonal components of the three-dimensional hydraulic conductivity full tensor. Furthermore, this study employs two-dimensional numerical simulations to examine the necessity of incorporating the full-hydraulic conductivity tensor when simulating seepage flow beneath a concrete dam, considering the varying degrees of stratigraphic inclination.

BACKGROUND

Darcy's law

If v_x, v_y and v_z are the components of Darcy's velocity ($\vec{v}$) – which represents the discharge velocity of groundwater flow in X, Y and Z directions, respectively – Darcy's law in the case of anisotropic soil takes the following form:

$$\vec{v} = -\underline{\underline{k}}\vec{\nabla}h, \tag{1}$$

which can be rewritten in the matrix form as follows:

$$\begin{bmatrix} v_x \\ v_y \\ v_z \end{bmatrix} = -\begin{bmatrix} k_{xx} & k_{xy} & k_{xz} \\ k_{yx} & k_{yy} & k_{yz} \\ k_{zx} & k_{zy} & k_{zz} \end{bmatrix} \begin{bmatrix} \frac{\partial}{\partial x} \\ \frac{\partial}{\partial y} \\ \frac{\partial}{\partial z} \end{bmatrix} h, \tag{2}$$

where:
h – total (hydraulic) head,
k_{xx}, k_{yy}, k_{zz} – diagonal elements,
k_{xy}, k_{xz}, k_{yx}, k_{yz}, k_{zx}, k_{zy} – nondiagonal elements of hydraulic conductivity tensor $\underline{\underline{k}}$; the nondiagonal elements of $\underline{\underline{k}}$ are symmetrical.

Seepage

In terms of the specific/elastic capacity (i.e., retention) of water (m_v) and temporal variations of the hydraulic head (h) for transient seepage equation (Fredlund & Rahardjo, 1993; Genetti Jr, 1999) can be written as follows:

$$\vec{\nabla}\vec{v} = -\frac{\partial\theta}{\partial t}, \tag{3}$$

where:
θ – volumetric water content.

For unsaturated soils with constant porosity temporal, the variations of θ, $(\frac{\partial \theta}{\partial t})$ can be written as $m_v \frac{\partial h}{\partial t}$, where m_v is the slope of the soil water-retention characteristics curve (SWRC). For the purpose of this paper, the SWRC is approximated to a two-segment polynomial with the two values for its slope, $m_v \approx 0.001$ m^{-1} for unsaturated soils and $m_v \approx 0.00001$ m^{-1} for saturated soils.

DERIVATION OF HYDRAULIC CONDUCTIVITY TENSOR

In general, the tensor $\underline{\underline{k}}$ has three categories of major (k_1), intermediate (k_2) and minor (k_3) principal hydraulic conductivity scalar values, where k_3 is normal and k_1 and k_2 are aligned within the soil stratigraphic plane. However, if there is a tilt in the stratigraphic planes due to natural deposition (e.g., tectonic plate movements) or human activity (e.g., tillage and field traffic), (Pulido-Moncada et al., 2021), the elements of $\underline{\underline{k}}$ that are not on the diagonal need to be taken into account (i.e., will be non-zero). Nevertheless, due to the mesoscale axisymmetry of the soil, typically, the equality of k_1 and k_2 exists within the stratigraphic planes. When analysing seepage in an orthogonal coordinate system aligned with the three principal orientations of the tensor (such as horizontal stratigraphic and XY planes), the tensor is diagonal; otherwise, the hydraulic conductivity tensor $\underline{\underline{k}}$ will be nondiagonal.

Two-dimensional hydraulic conductivity tensor

In a two-dimensional system of coordinates XZ and the stratigraphic plane with a positive slope α (i.e., the tilt angle is above X axis), the components of the hydraulic conductivity tensor $\underline{\underline{k}}$ (k_{xx}, k_{zz}, k_{xz} , k_{zx}) are computed in terms of k_1 and k_3 as follows:

$$k_{xx} = \left(\frac{k_1+k_3}{2}\right) + \left(\frac{k_1-k_3}{2}\right)\cos 2\alpha, \tag{4a}$$

$$k_{xz} = k_{zx} = \left(\frac{k_1-k_3}{2}\right)\sin 2\alpha, \tag{4b}$$

$$k_{zz} = \left(\frac{k_1+k_3}{2}\right) - \left(\frac{k_1-k_3}{2}\right)\cos 2\alpha. \tag{4c}$$

Derivation of three-dimensional hydraulic conductivity tensor

In the case of the three-dimensional system of coordinates XYZ, Darcy's velocity equation represented by Eq. (2) can be rewritten as follows:

$$v_x = k_{xx}\, g_x + k_{xy}\, g_y + k_{xz}\, g_z, \tag{5a}$$

$$v_y = k_{yx}\, g_x + k_{yy}\, g_y + k_{yz}\, g_z, \tag{5b}$$

$$v_z = k_{zx}\, g_x + k_{zy}\ \ g_y + k_{zz}\, g_z, \tag{5c}$$

where:

$g_x = -\frac{\partial h}{\partial x}$, $g_y = -\frac{\partial h}{\partial y}$ and $g_z = -\frac{\partial h}{\partial z}$.

Suppose orthogonal unit vectors $\overrightarrow{a_1}$, $\overrightarrow{a_2}$ and $\overrightarrow{a_3}$ and velocity vectors $\overrightarrow{v_1}$, $\overrightarrow{v_2}$ and $\overrightarrow{v_3}$ are in the orientation of k_1, k_2 and k_3, Darcy's velocity $\vec{v}$ can then also take the following form:

$$\vec{v} = v_1\overrightarrow{a_1} + v_2\overrightarrow{a_2} + v_3\overrightarrow{a_3}, \tag{6}$$

where:
$\overrightarrow{a_1} = a_{1x}\hat{\imath} + a_{1y}\hat{\jmath} + a_{1z}\hat{k}$, $\overrightarrow{a_2} = a_{2x}\hat{\imath} + a_{2y}\hat{\jmath} + a_{2z}\hat{k}$ and $\overrightarrow{a_3} = a_{3x}\hat{\imath} + a_{3y}\hat{\jmath} + a_{3z}\hat{k}$,
$\hat{\imath}$, $\hat{\jmath}$, $\hat{k}$ – unit vectors along the X, Y and Z axes.

If the positive values of g_x, g_y and g_z are projected on the k_1, k_2 and k_3 axes, then the flow velocity $\overrightarrow{v_1}$ along the 1, 2 and 3 directions can be simplified as follows.

$$v_1 = (v_1)_{g_x} + (v_1)_{g_y} + (v_1)_{g_z}, \tag{7}$$

where:

$$(v_1)_{g_x} = [(g_x\hat{\imath}) \cdot \overrightarrow{a_1}]k_1 = \left[(g_x\hat{\imath}) \cdot \left(a_{1x}\hat{\imath} + a_{1y}\hat{\jmath} + a_{1z}\hat{k}\right)\right]k_1 = g_x a_{1x} k_1, \tag{8a}$$

$$(v_1)_{g_y} = \left[\left(g_y\hat{\jmath}\right) \cdot \overrightarrow{a_1}\right]k_1 = \left[\left(g_y\hat{\jmath}\right) \cdot \left(a_{1x}\hat{\imath} + a_{1y}\hat{\jmath} + a_{1z}\hat{k}\right)\right]k_1 = g_y a_{1y} k_1, \tag{8b}$$

$$(v_1)_{g_z} = \left[\left(g_z\hat{k}\right) \cdot \overrightarrow{a_1}\right]k_1 = \left[\left(g_z\hat{k}\right) \cdot \left(a_{1x}\hat{\imath} + a_{1y}\hat{\jmath} + a_{1z}\hat{k}\right)\right]k_1 = g_z a_{1z} k_1. \tag{8c}$$

Substitution of these values on Eq. (7) reduces to the following form:

$$v_1 = \left(g_x a_{1x} + g_y a_{1y} + g_z a_{1z}\right)k_1. \tag{9}$$

In a similar manner:

$$v_2 = \left(g_x a_{2x} + g_y a_{2y} + g_z a_{2z}\right)k_2, \tag{10}$$

$$v_3 = \left(g_x a_{3x} + g_y a_{3y} + g_z a_{3z}\right)k_3. \tag{11}$$

Employing Eq. (9) through Eq. (11) on Eq. (6) and rearranging results as follows:

$$\begin{aligned}\vec{v} = &\left[\left(g_x {a_{1x}}^2 + g_y a_{1x}a_{1y} + g_z a_{1x}a_{1z}\right)k_1 + \left(g_x {a_{2x}}^2 + g_y a_{2x}a_{2y} + g_z a_{2x}a_{2z}\right)k_2 + \left(g_x {a_{3x}}^2 + \right.\right. \\ &\left.\left. + g_y a_{3x}a_{3y} + g_z a_{3x}a_{3z}\right)k_3\right]\hat{\imath} + \left[\left(g_x a_{1y}a_{1x} + g_y {a_{1y}}^2 + g_z a_{1y}a_{1z}\right)k_1 + \left(g_x a_{2y}a_{2x} + g_y {a_{2y}}^2 + \right.\right. \\ &\left.\left. + g_z a_{2y}a_{2z}\right)k_2 + \left(g_x a_{3y}a_{3x} + g_y {a_{3y}}^2 + g_z a_{3y}a_{3z}\right)k_3\right]\hat{\jmath} + \left[\left(g_x a_{1z}a_{1x} + g_y a_{1z}a_{1y} + g_z {a_{1z}}^2\right)k_1 + \right. \\ &\left. + \left(g_x a_{2z}a_{2x} + g_y a_{2z}a_{2y} + g_z {a_{2z}}^2\right)k_2 + \left(g_x a_{3z}a_{3x} + g_y a_{3z}a_{3y} + g_z {a_{3z}}^2\right)k_3\right]\hat{k}.\end{aligned} \tag{12}$$

Comparing Eq. (12) with $\vec{v} = v_x\hat{\imath} + v_y\hat{\jmath} + v_z\hat{k}$ results in:

$$v_x = ({a_{1x}}^2 k_1 + {a_{2x}}^2 k_2 + {a_{3x}}^2 k_3)g_x + \left(a_{1x}a_{1y}k_1 + a_{2x}a_{2y}k_2 + a_{3x}a_{3y}k_3\right)g_y + (a_{1x}a_{1z}k_1 + \\ + a_{2x}a_{2z}k_2 + a_{3x}a_{3z}k_3)g_z, \tag{13a}$$

$$v_y = \left(a_{1y}a_{1x}k_1 + a_{2y}a_{2x}k_2 + a_{3y}a_{3x}k_3\right)g_x + \left({a_{1y}}^2 k_1 + {a_{2y}}^2 k_2 + {a_{3y}}^2 k_3\right)g_y + \left(a_{1y}a_{1z}k_1 + \\ + a_{2y}a_{2z}k_2 + a_{3y}a_{3z}k_3\right)g_z, \tag{13b}$$

$$v_z = (a_{1z}a_{1x}k_1 + a_{2z}a_{2x}k_2 + a_{3z}a_{3x}k_3)g_x + \left(a_{1z}a_{1y}k_1 + a_{2z}a_{2y}k_2 + a_{3z}a_{3y}k_3\right)g_y + \\ + ({a_{1z}}^2 k_1 + {a_{2z}}^2 k_2 + {a_{3z}}^2 k_3)g_z. \tag{13c}$$

Equating the left-hand sides of Eq. (5) with Eq. (13) provides the diagonal and nondiagonal components of the hydraulic conductivity tensor $\underline{\underline{k}}$ in terms of k_1, k_2 and k_3 as follows:

$$\left.\begin{aligned} k_{xx} &= {a_{1x}}^2 k_1 + {a_{2x}}^2 k_2 + {a_{3x}}^2 k_3 \\ k_{yy} &= {a_{1y}}^2 k_1 + {a_{2y}}^2 k_2 + {a_{3y}}^2 k_3 \\ k_{zz} &= {a_{1z}}^2 k_1 + {a_{2z}}^2 k_2 + {a_{3z}}^2 k_3 \\ k_{xy} = k_{yx} &= a_{1x}a_{1y}k_1 + a_{2x}a_{2y}k_2 + a_{3x}a_{3y}k_3 \\ k_{yz} = k_{zy} &= a_{1y}a_{1z}k_1 + a_{2y}a_{2z}k_2 + a_{3y}a_{3z}k_3 \\ k_{zx} = k_{xz} &= a_{1z}a_{1x}k_1 + a_{2z}a_{2x}k_2 + a_{3z}a_{3x}k_3 \end{aligned}\right\} \tag{14}$$

The unit vectors $\overrightarrow{a_1}$, $\overrightarrow{a_2}$ and $\overrightarrow{a_3}$ are orthogonal to each other and $\overrightarrow{a_3}$ is normal to the soil stratigraphic plane (Fig. 1). The figure shows the projection of $\overrightarrow{a_3}$ and $\overrightarrow{a_1}$ on the X, Y and Z axes, respectively – from which the unit vectors $\overrightarrow{a_1}$, $\overrightarrow{a_2}$ and $\overrightarrow{a_3}$ can be expressed in terms of the vertical angle and azimuth.

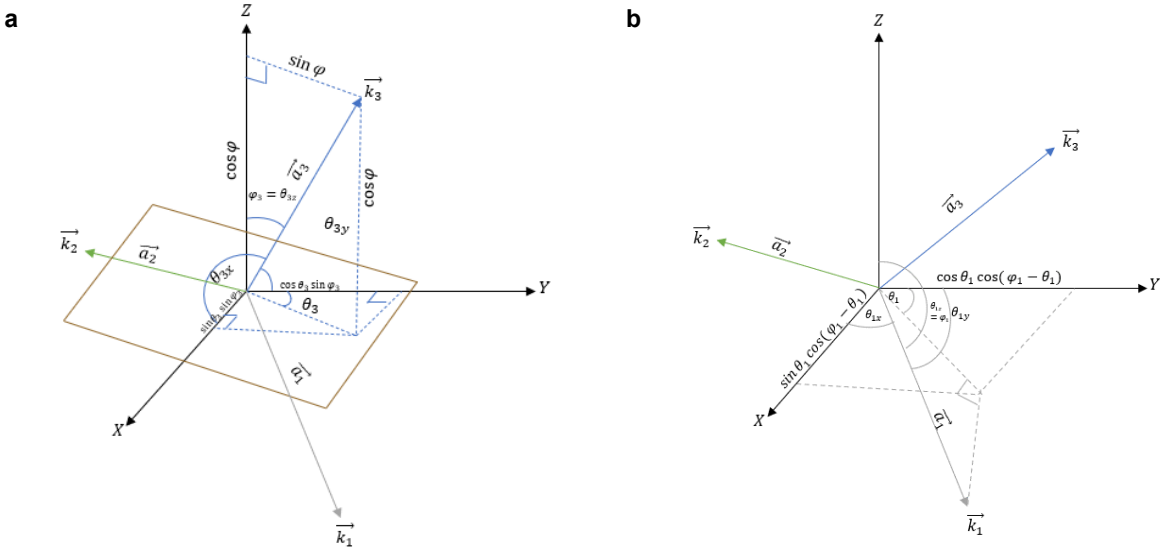

Fig. 1. Projections: a – $\overrightarrow{a_3}$ on X, Y and Z axes; b – $\overrightarrow{a_1}$ on X, Y and Z axes

Source: authors' compilation.

Assuming unit vectors $\overrightarrow{a_1}$, $\overrightarrow{a_2}$ and $\overrightarrow{a_3}$ can be expressed as follows:

$$\overrightarrow{a_1} = a_{1x}\hat{\imath} + a_{1y}\hat{\jmath} + a_{1z}\hat{k} = \cos\theta_{1x}\,\hat{\imath} + \cos\theta_{1y}\,\hat{\jmath} + \cos\theta_{1z}\,\hat{k}, \tag{15a}$$

$$\overrightarrow{a_2} = a_{2x}\hat{\imath} + a_{2y}\hat{\jmath} + a_{2z}\hat{k} = \cos\theta_{2x}\,\hat{\imath} + \cos\theta_{2y}\,\hat{\jmath} + \cos\theta_{2z}\,\hat{k}, \tag{15b}$$

$$\overrightarrow{a_3} = a_{3x}\hat{\imath} + a_{3y}\hat{\jmath} + a_{3z}\hat{k} = \cos\theta_{3x}\,\hat{\imath} + \cos\theta_{3y}\,\hat{\jmath} + \cos\theta_{3z}\,\hat{k}. \tag{15c}$$

From Figure 1a, it can be concluded that:

$$\overrightarrow{a_3} = \cos\theta_{3x}\,\hat{\imath} + \cos\theta_{3y}\,\hat{\jmath} + \cos\theta_{3z}\,\hat{k} \Rightarrow \overrightarrow{a_3} = \sin\theta_3 \sin\varphi_3\,\hat{\imath} + \cos\theta_3 \sin\varphi_3\,\hat{\jmath} + \cos\varphi_3\,\hat{k}. \tag{16}$$

For any given vertical angle (VA), where $\varphi_3 = (90° - VA)$; and azimuth A_{z3}, where $\theta_3 = A_{z3}$, $\overrightarrow{a_3}$ can be found from Eq. (16).

Similarly, from Figure 1b, it can be deduced that:

$$\overrightarrow{a_1} = \cos\theta_{1x}\,\hat{\imath} + \cos\theta_{1y}\,\hat{\jmath} + \cos\theta_{1z}\,\hat{k} \Rightarrow \overrightarrow{a_1} = \sin\theta_1 \cos(\varphi_1 - \theta_1)\,\hat{\imath} + \\ + \cos\theta_1 \cos(\varphi_1 - \theta_1)\,\hat{\jmath} + \cos\varphi_1\,\hat{k}. \tag{17}$$

Since $\overrightarrow{a_1}$ and $\overrightarrow{a_3}$ are orthogonal, their dot product is zero (i.e., $\overrightarrow{a_1} \cdot \overrightarrow{a_3} = 0$), which is essentially the dot product of Eq. (16) and (17) results in the following form.

$$\sin\theta_1 \cos(\varphi_1 - \theta_1) \sin\theta_3 \sin\varphi_3 + \cos\theta_1 \cos(\varphi_1 - \theta_1) \cos\theta_3 \sin\varphi_3 + \cos\varphi_1 \cos\varphi_3 = 0. \tag{18}$$

For a given azimuth A_{z1}, where $\theta_1 = A_{z1}$, the value of $\varphi_1, 0 < \varphi_1 < \pi$ can be found from Eq. (18) to obtain $\overrightarrow{a_1}$ from Eq. (17).

Again, since $\overrightarrow{a_2}$ is orthogonal to both $\overrightarrow{a_1}$ and $\overrightarrow{a_3}$; therefore, $\overrightarrow{a_2} = \overrightarrow{a_1} \times \overrightarrow{a_3}$. Thus, the cross-product of Eq. (16) and Eq. (17) produces $\overrightarrow{a_2}$ as follows:

$$\overrightarrow{a_2} = (\cos\theta_1 \cos(\varphi_1 - \theta_1) \cos\varphi_3 - \cos\varphi_1 \cos\theta_3 \sin\varphi_3)\hat{\imath} + (\cos\varphi_1 \sin\theta_3 \sin\varphi_3 - \sin\theta_1 \cos(\varphi_1 - \\ - \theta_1) \cos\varphi_3)\,\hat{\jmath} + (\sin\theta_1 \cos(\varphi_1 - \theta_1) \cos\theta_3 \sin\varphi_3 - \cos\theta_1 \cos(\varphi_1 - \theta_1) \sin\theta_3 \sin\varphi_3)\hat{k}. \tag{19}$$

Substituting Eqs (16), (17) and (19) into Eq. (14) gives the elements of the full three-dimensional hydraulic conductivity tensor $\underline{\underline{k}}$ as follows:

$$k_{xx} = \sin^2\theta_1 \cos^2(\varphi_1 - \theta_1)\,k_1 + (\cos\theta_1 \cos(\varphi_1 - \theta_1) \cos\varphi_3 - \cos\varphi_1 \cos\theta_3 \sin\varphi_3)^2 k_2 + \\ + \sin^2\theta_3 \sin^2\varphi_3\,k_3, \tag{20a}$$

$$k_{yy} = \cos^2\theta_1 \cos^2(\varphi_1 - \theta_1)\,k_1 + (\cos\varphi_1 \sin\theta_3 \sin\varphi_3 - \sin\theta_1 \cos(\varphi_1 - \theta_1) \cos\varphi_3)^2\,k_2 + \\ + \cos^2\theta_3 \sin^2\varphi_3\,k_3, \tag{20b}$$

$$k_{zz} = \cos^2\varphi_1\,k_1 + (\sin\theta_1 \cos(\varphi_1 - \theta_1) \cos\theta_3 \sin\varphi_3 - \cos\theta_1 \cos(\varphi_1 - \theta_1) \sin\theta_3 \sin\varphi_3)^2 k_2 + \\ + \cos^2{\varphi_3}^2\,k_3, \tag{20c}$$

$$k_{xy} = k_{yx} = \sin\theta_1 \cos\theta_1 \cos^2(\varphi_1 - \theta_1)\, k_1 + (\cos\theta_1 \cos(\varphi_1 - \theta_1) \cos\varphi_3 - \\ - \cos\varphi_1 \cos\theta_3 \sin\varphi_3)(\cos\varphi_1 \sin\theta_3 \sin\varphi_3 - \sin\theta_1 \cos(\varphi_1 - \theta_1) \cos\varphi_3)\, k_2 + \\ + \sin\theta_3 \sin\varphi_3 \cos\theta_3 \sin\varphi_3\, k_3, \tag{20d}$$

$$k_{yz} = k_{zy} = \cos\theta_1 \cos(\varphi_1 - \theta_1) \cos\varphi_1\, k_1 + (\cos\varphi_1 \sin\theta_3 \sin\varphi_3 - \sin\theta_1 \cos(\varphi_1 - \\ - \theta_1) \cos\varphi_3)\ (\sin\theta_1 \cos(\varphi_1 - \theta_1) \cos\theta_3 \sin\varphi_3 - \cos\theta_1 \cos(\varphi_1 - \theta_1) \sin\theta_3 \sin\varphi_3)\, k_2 + \\ + \cos\theta_3 \sin\varphi_3 \cos\varphi_3\, k_3, \tag{20e}$$

$$k_{zx} = k_{xz} = \cos\varphi_1 \sin\theta_1 \cos(\varphi_1 - \theta_1) k_1 + (\sin\theta_1 \cos(\varphi_1 - \theta_1) \cos\theta_3 \sin\varphi_3 - \cos\theta_1 \cos(\varphi_1 - \\ - \theta_1) \sin\theta_3 \sin\varphi_3)(\cos\theta_1 \cos(\varphi_1 - \theta_1) \cos\varphi_3 - \cos\varphi_1 \cos\theta_3 \sin\varphi_3) k_2 + \cos\varphi_3 \sin\theta_3 \sin\varphi_3\, k_3. \tag{20f}$$

NUMERICAL SIMULATION

Seepage flow formulation

The seepage flow under a concrete dam is simulated here to demonstrate the impact of the nondiagonal $\underline{\underline{k}}$ on the tilted soil's stratigraphic planes. In this model, the upstream and downstream lakes are simulated as inlet and outlet, respectively – as schematically shown in Figure 2.

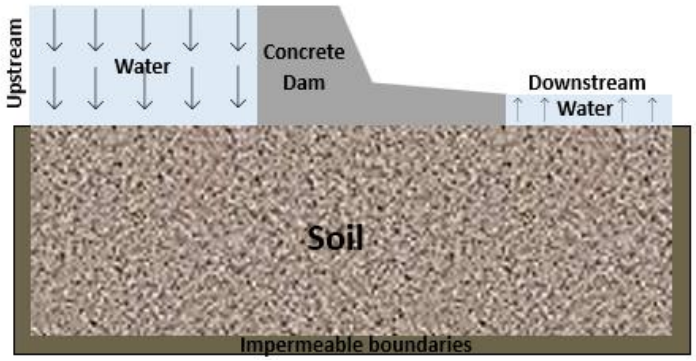

Fig. 2. Schematic of the model for an upstream (inlet) and a downstream (outlet) at the top boundary

Source: authors' compilation.

Mathematical model

The combination of Eq. (1) and Eq. (2) govern the seepage, which for a two-dimensional problem can be reduced to the following form:

$$-\begin{bmatrix}\frac{\partial}{\partial x} & \frac{\partial}{\partial z}\end{bmatrix}\begin{bmatrix}k_{xx} & k_{xz}\\ k_{zx} & k_{zz}\end{bmatrix}\begin{bmatrix}\frac{\partial}{\partial x}\\ \frac{\partial}{\partial z}\end{bmatrix} h = -m_v \frac{\partial h}{\partial t}, \tag{21}$$

which can be expanded as follows:

$$-\left[\frac{\partial k_{xx}}{\partial x}\frac{\partial h}{\partial x} + k_{xx}\frac{\partial^2 h}{\partial x^2} + \frac{\partial k_{xz}}{\partial x}\frac{\partial h}{\partial z} + k_{xz}\frac{\partial^2 h}{\partial x \partial z} + \frac{\partial k_{zx}}{\partial z}\frac{\partial h}{\partial x} + k_{zx}\frac{\partial^2 h}{\partial z \partial x} + \frac{\partial k_{zz}}{\partial z}\frac{\partial h}{\partial z} + k_{zz}\frac{\partial^2 h}{\partial z^2}\right] = -m_v \frac{\partial h}{\partial t}. \tag{22}$$

Finite-difference model development

A two-dimensional finite-difference numerical model was developed using the MATLAB interface, with Dirichlet boundary conditions at the upstream (inlet) and downstream (outlet) (i.e., hydraulic heads are constants (H_1 and H_2) and Neumann boundary conditions considered for the rest of the impermeable boundaries). This model is used to demonstrate that in the case of tilted soil stratigraphic planes, the full--hydraulic conductivity tensor $\underline{\underline{k}}$ is required to simulate seepage flow accurately.

The linearised form of Eq. (22), discretised over a rectangular grid using the forward finite difference for first-order derivatives and central finite difference for higher-order derivatives, can be shown as:

$$\frac{k_{xx(i,j)}}{(\Delta x)^2} h_{i,j-1}^{t_{k+1}} - \left(\frac{k_{xx(i,j+1)}-k_{xx(i,j)}}{(\Delta x)^2} + 2\frac{k_{xx(i,j)}}{(\Delta x)^2} + \frac{k_{xz(i,j+1)}-k_{xz(i,j)}}{\Delta x \Delta z} + 2\frac{k_{xz(i,j)}}{\Delta x \Delta z} + \frac{k_{zx(i+1,j)}-k_{zx(i,j)}}{\Delta z \Delta x} + 2\frac{k_{zx(i,j)}}{\Delta z \Delta x} + \right.$$
$$+ \frac{k_{zz(i+1,j)}-k_{zz(i,j)}}{(\Delta z)^2} + 2\frac{k_{zz(i,j)}}{(\Delta z)^2} + \left.\frac{m_{v(i,j)}}{\Delta t}\right) h_{i,j}^{t_{k+1}} + \left(\frac{k_{xx(i,j+1)}-k_{xx(i,j)}}{(\Delta x)^2} + \frac{k_{xx(i,j)}}{(\Delta x)^2} + \frac{k_{zx(i+1,j)}-k_{zx(i,j)}}{\Delta z \Delta x}\right) h_{i,j+1}^{t_{k+1}} +$$
$$+ \left(\frac{k_{xz(i,j)}}{\Delta x \Delta z} + \frac{k_{zx(i,j)}}{\Delta z \Delta x}\right) h_{i-1,j-1}^{t_{k+1}} + \frac{k_{zz(i,j)}}{(\Delta z)^2} h_{i-1,j}^{t_{k+1}} + \left(\frac{k_{xz(i,j+1)}-k_{xz(i,j)}}{\Delta x \Delta z} + \frac{k_{zz(i+1,j)}-k_{zz(i,j)}}{(\Delta z)^2} + \frac{k_{zz(i,j)}}{(\Delta z)^2}\right) h_{i+1,j}^{t_{k+1}} +$$
$$+ \left(\frac{k_{xz(i,j)}}{\Delta x \Delta z} + \frac{k_{zx(i,j)}}{\Delta z \Delta x}\right) h_{i+1,j+1}^{t_{k+1}} = -\frac{m_{v(i,j)}}{\Delta t} h_{i,j}^{t_k}, \tag{23}$$

where $h_{i,j}^{t_k}$ represents the hydraulic head on Row i, Column j (i.e., Node (i,j)) in the space and at time instance t_k; $h_{i,j}^{t_{k+1}}$ is the hydraulic head at Node (i,j) at time t_{k+1} and so on. For this model, in the case of unsaturated soil – with each time step – each of the components of the $\underline{\underline{k}}$ in Eq. (23) were updated using the soil water-retention formula (Alam & Farid, 2023), which introduces nonlinearity back into the equation. Thus, these nonlinear components of the $\underline{\underline{k}}$ were updated using a modified iterated Crank–Nicholson scheme (Tran & Liu, 2016) until they converged to their optimal value.

Simulation result and discussion

The subsequent conditions were applied for every scenario shown in Figures 3–5. The soil is initially unsaturated, with a total head of $h = 0$, indicating capillary rise and suction at all elevations. All other soil boundaries, apart from inlets and outlets, are impermeable. The assumed dimensions of the soil are 30 m for the horizontal length (L) and 10 m for the vertical length – thickness (T). The initial hydraulic heads at the inlet is $H_1 = 50$ m, and at the outlet, $H_2 = 10$ m. The seepage flow is simulated through an anisotropic soil with a major principal hydraulic conductivity value of $k_1 = 5.5 \times 10^{-2}$ m·s^{-1} and a minor principal hydraulic conductivity value of $k_3 = 1.5 \times 10^{-2}$ m·s^{-1} of the hydraulic conductivity tensor $\underline{\underline{k}}$. Each scenario was examined for 5,000 s at a time step of $\Delta t = 20$ s.

The model was tested for various additional circumstances; however, only a few are shown below. In all of the following scenarios, a tilt is present, resulting in estimated values of the diagonal components of the hydraulic conductivity tensor as $k_{xx} = 5.03 \times 10^{-2}$ m·s^{-1} $< k_1$ and $k_{zz} = 1.97 \times$ $\times 10^{-2}$ m·s^{-1} $> k_3$. In Figure 3, the first scenario, however, inaccurately depicts a symmetric seepage flow pattern identical for both downward ($\alpha = -20°$) and upward ($\alpha = 20°$) tilts due to erroneous assumption of the values of the nondiagonal components of the tensor $\underline{\underline{k}}$ as $k_{xz} = k_{zx} = 0$. However, for $\alpha = -20°$ and $\alpha = 20°$, Figures 4 and 5 exhibit accurate seepage flow patterns, with calculated values for the nondiagonal components as $k_{xz} = k_{zx} = -1.29 \times 10^{-2}$ m·s^{-1} and $k_{xz} = k_{zx} = 1.29 \times 10^{-2}$ m·s^{-1}, consequently.

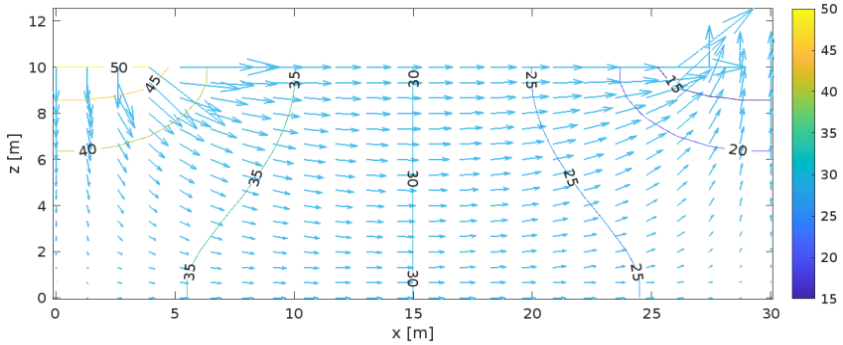

Fig. 3. Equipotential lines and flow velocity vectors considering a forced diagonalised (erroneous approximation) hydraulic conductivity tensor (i.e., $k_{xz} = k_{zx} = 0$), which has produced the same results for tilts (between the soil stratigraphic plane and the horizontal X axis) of α = 20° (i.e., above the horizon) and α = –20° (i.e., below the horizon)

Source: authors' compilation.

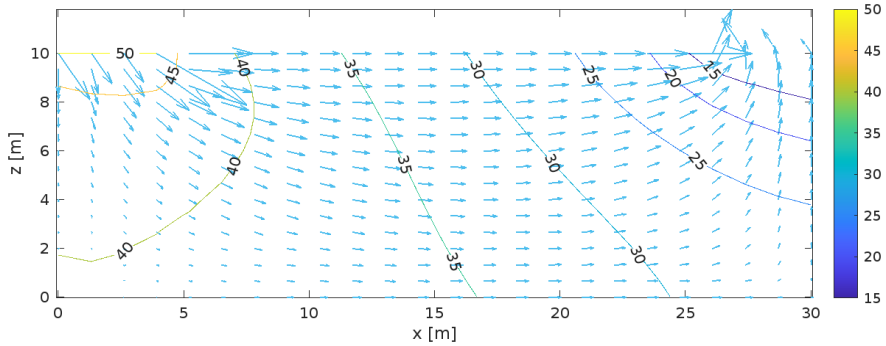

Fig. 4. Equipotential lines and flow velocity vectors for nondiagonalised (correct approximation) hydraulic conductivity tensor (i.e., $k_{xz} = k_{zx} \neq 0$) for a tilt between the soil stratigraphic plane and horizontal X-axis with slope α = –20° (i.e., below the horizon)

Source: authors' compilation.

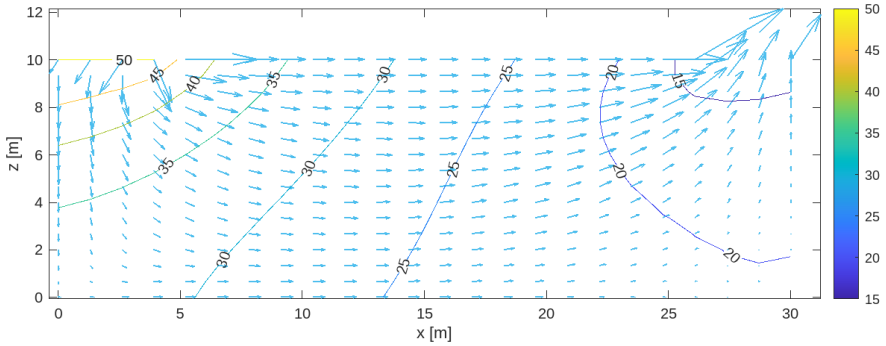

Fig. 5. Equipotential lines and flow velocity vectors for non-diagonalised (correct approximation) hydraulic conductivity tensor (i.e., $k_{xz} = k_{zx} \neq 0$) for a tilt between the soil stratigraphic plane and the horizontal X-axis with slope α = 20° (i.e., above the horizon)

Source: authors' compilation.

CONCLUSIONS

This study introduces formulas to compute three-dimensional full-hydraulic conductivity tensor components. Furthermore, seepage flow under a concrete dam is simulated using a two-dimensional finite-difference numerical model to illustrate the failure of ignoring the nondiagonal components of the hydraulic conductivity tensor inaccurately finding seepage flow for scenarios that involve tilted soil stratigraphic planes. Although the provided formula analytically calculates both diagonal and nondiagonal elements of the three-dimensional full-hydraulic conductivity tensor, there is still a need to develop a three-dimensional model for simulating seepage flow that can employ the three-dimensional full-hydraulic conductivity tensor to replicate realistic circumstances, enabling an exhaustive evaluation of the formula's precision.

Authors' contributions

Conceptualisation: M.A. and A.F.; methodology: M.A.; validation: A.F. and Y.Y.; formal analysis: M.A. and A.F.; investigation: M.A.; resources: M.A. and A.F.; data curation: M.A. and A.F.; writing – original draft preparation: M.A.; writing – review and editing: A.F.; visualisation: M.A.; supervision: A.F.; project administration: A.F.; funding acquisition: A.F.

All authors have read and agreed to the published version of the manuscript.

REFERENCES

Alam, M. K. & Farid, A. (2023). Impact of nondiagonal elements of hydraulic conductivity tensor on seepage through anisotropic soils. *9th International Congress on Environmental Geotechnics*, *3*, 124–134. Chania, Greece: ISSMGE. https://doi.org/10.53243/ICEG2023-147

Assouline, S. & Or, D. (2006). Anisotropy factor of saturated and unsaturated soils. *Water Resources Research*, *42* (12). https://doi.org/10.1029/2006WR005001

Ertekin, T., Abou-Kassem, J. H. & King, G. R. (2001). *Basic Applied Reservoir Simulation*. Richardson: Society of Petroleum Engineers.

Fanchi, J. R. (2005). *Principles of Applied Reservoir Simulation*. Elsevier.

Fanchi, J. R. (2008). Directional Permeability. *SPE Reservoir Evaluation & Engineering*, *11* (03), 565–568. https://doi.org/10.2118/102343-PA

Fredlund, D. G. & Rahardjo, H. (1993). *Soil Mechanics for Unsaturated Soils*. John Wiley & Sons.

Genetti Jr, A. J. (1999). *Groundwater Hydrology*. Washington DC: Corps of Engineers.

Nguyen, H. B. K., Rahman, M. M. & Karim, M. R. (2023). Effect of soil anisotropy and variability on the stability of undrained soil slope. *Frontiers in Built Environment*, *9*. https://doi.org/10.3389/fbuil.2023.1117858

Peng, X. (2011). Anisotropy of soil physical properties. In J. Gliński, J. Horabik, J. Lipiec (Eds), *Encyclopedia of Agrophysics* (pp. 55–57). Dordrecht: Springer. https://doi.org/10.1007/978-90-481-3585-1_15

Pulido-Moncada, M., Labouriau, R., Kesser, M., Zanini, P. P. G., Guimarães, R. M. L. & Munkholm, L. J. (2021). Anisotropy of subsoil pore characteristics and hydraulic conductivity as affected by compaction and cover crop treatments. *Soil Science Society of America Journal*, *85* (1), 28–39. https://doi.org/10.1002/saj2.20134

Tran, Q. & Liu, J. (2016, July 22). *Modified Iterated Crank-Nicolson Method with Improved Accuracy*. arXiv. https://doi.org/10.48550/arXiv.1608.01344

Alam, M. K., Farid, A. (2024). Hydraulic conductivity tensor of anisotropic soils: the impact on seepage flow. *Acta Sci. Pol. Architectura*, *23*, 1–11, DOI: 10.22630/ASPA.2024.23.1

WYZNACZANIE TENSORA PEŁNEGO PRZEWODNICTWA HYDRAULICZNEGO GRUNTU ANIZOTROPOWEGO: WPŁYW NA PRZEPŁYW WYCIEKÓW POD ZAPORĄ BETONOWĄ

STRESZCZENIE

Naturalne lub sztuczne zmiany w orientacji płaszczyzny stratygraficznej gleby (tj. osadzanie się gleby i osadów w odrębnych warstwach) mogą powodować zmiany przewodności hydraulicznej w zależności od kierunku pomiaru. Z tego powodu należy uwzględnić w tym przypadku przewodność hydrauliczną jako niediagonalny pełny tensor, aby odpowiednio przedstawić wpływ orientacji płaszczyzn stratygraficznych gleby na wzór przepływu infiltracyjnego. W niniejszej pracy przedstawiono wzór na trójwymiarowe niediagonalne obliczenie tensora pełnego przewodnictwa hydraulicznego w aspekcie azymutu i kąta pionowego. Ponadto przedstawiono symulacje numeryczne dwuwymiarowych przepływów wyciekowych pod betonową zaporą, aby wykazać potrzebę uwzględnienia pełnego tensora przewodności hydraulicznej dla różnych stopni nachylenia stratygraficznego względem układu współrzędnych.

Słowa kluczowe: pełny tensor, przewodność hydrauliczna, przepływ przesiąkający, stratygrafia gleby, model numeryczny